

Uncertainty Prediction for Deep Sequential Regression Using Meta Models

Jiří Navrátil¹ Matthew Arnold¹ Benjamin Elder¹

Abstract

Generating high quality uncertainty estimates for sequential regression, particularly deep recurrent networks, remains a challenging and open problem. Existing approaches often make restrictive assumptions (such as stationarity) yet still perform poorly in practice, particularly in presence of real world non-stationary signals and drift. This paper describes a flexible method that can generate symmetric and asymmetric uncertainty estimates, makes no assumptions about stationarity, and outperforms competitive baselines on both drift and non drift scenarios. This work helps make sequential regression more effective and practical for use in real-world applications, and is a powerful new addition to the modeling toolbox for sequential uncertainty quantification in general.

1. Introduction

The ability to quantify the uncertainty of a model is one of the fundamental requirements in trusted, safe, and actionable AI (Arnold et al., 2019; Jiang et al., 2018; Begoli et al., 2019).

This paper focuses on uncertainty quantification in regression tasks, particularly in the context of deep neural networks (DNN). We define a sequential task as one involving an ordered series of input elements, represented by features, and an ordered series of outputs. In sequential *regression* tasks (SRT), the output elements are (possibly multivariate) real-valued variables. SRT occur in numerous applications, among others, in weather modeling, environmental modeling, energy optimization, and medical and biotechnology applications. When the cost of making an incorrect prediction is particularly high, such as in human safety, medical decisions or high-investment resource exploration, models without a reliable uncertainty estimation are perceived high risk and may not be adopted.

Uncertainty prediction in DNNs has been subject to ac-

tive research, in particular, spurred by what has become known as the “Overconfidence Problem” of DNNs (Guo et al., 2017), and by their susceptibility to adversarial attacks (Madry et al., 2017). However, the bulk of work is concerned with non-sequential, classification tasks (see Section 2) leaving a noticeable gap for SRT. Furthermore, unlike with classification, the uncertainty evaluation methodology for SRT remains rather undeveloped.

In this paper we introduce a meta-modeling concept as an approach to achieving high-quality uncertainty quantification in DNNs for SRT. We demonstrate that it not only outperforms competitive baselines but also provides consistent results across a variety of drift scenarios. We believe the approach represents a new powerful addition to the modeling toolbox in general.

The novel contributions of this paper are summarized as follows:

- Application of the meta-modeling concept to SRT
- Developing a *joint* base-meta model and its comparison to white- and black-box alternatives
- Generating *asymmetric* uncertainty bounds in DNNs
- Proposing a new evaluation methodology for SRT

2. Related Work

Classical statistics on time series offers an abundance of work dealing with uncertainty quantification (Papoulis & Saunders, 1989). Most notably in econometrics, a variety of heteroskedastic variance models lead to highly successful application in financial market volatility analyses (Engle, 1982; Bollerslev, 1986; Mills, 1991). An Autoregressive Conditional Heteroskedastic, or ARCH, model (Engle, 1982), and its generalized version, GARCH, (Bollerslev, 1986) are two such methods. They assume an autoregressive moving-average, or ARMA, model to underlie the variance series. Besides its stationarity assumptions, long horizon forecasting using (G)ARCH is difficult (Starica et al., 2005; Chen & Politis, 2019) and is typically used in a one-step-ahead setting. We use the GARCH as one of our baselines.

Bayesian modeling is a probabilistic approach that naturally integrates the notion of uncertainty. An illuminating

¹IBM Research, Yorktown Heights, New York, USA. Correspondence to: Jiří Navrátil <jiri@us.ibm.com>.

study in image recognition (Kendall & Gal, 2017) describes an integration of two sources of uncertainty, namely the *epistemic* (due to model) and the *aleatoric* (due to data). The authors propose an approach utilizing a variational approximation of Bayesian Neural Networks and an implicit Gaussian model to quantify both types of variability in a non-sequential classification and regression task. The study, however, does not offer a comparison of different methods generating uncertainty. Based on (Nix & Weigend, 1994), (Lakshminarayanan et al., 2017) also uses a Gaussian variance integrated in a negative log-likelihood training objective with the aim at improving the predictive performance of the base model, again in a non-sequential setting. Similar to (Kendall & Gal, 2017), the study does not focus on comparing the quality of the uncertainty to other methods. We use the implicit variance model of (Kendall & Gal, 2017; Oh et al., 2020; Lakshminarayanan et al., 2017), as well as the method of variational dropout of (Gal & Ghahramani, 2016; Kendall & Gal, 2017) as baselines in our work. A meta-modeling approach was taken in (Chen et al., 2019) aiming at the task of instance filtering using white-box models. The work relates to ours through the meta-modeling concept but concentrates on classification in a non-sequential setting. Besides its application in filtering, meta-modeling has been widely applied in the task of learning to learn and lifelong learning (Schmidhuber, 1987; Finn et al., 2019). Uncertainty in data drift conditions was assessed in a recent study (Snoek et al., 2019). The authors employ calibration-based metrics to examine various methods for uncertainty in classification tasks (image and text data), and conclude, among others that most methods’ quality degrades with drift. Acknowledging drift as an important experimental aspect, our study takes it into account by defining matched and drifted scenarios. (Shen et al., 2018) described a multi-objective training of a DNN in wind power prediction, minimizing two types of cost related to coverage and bandwidth. We expand on these metrics in Section 3.3.1.

3. Method

3.1. Meta Modeling Approach

The basic concept of Meta Modeling (MM), depicted in Figure 1, involves a combination of two models comprising a *base model*, performing the main task (e.g., regression), and a *meta model*, learning to predict the base model’s error behavior. Depending on the amount of information shared between these two, we distinguish several settings, namely (1) base model is a black-box (BB), (2) base is a white-box (WB, base parameters are accessible), and (3) base and meta components are merged and trained jointly (JM). The advantages of WB and JM are obvious: rich information is available for the meta model to capture salient patterns for it to generate accurate predictions. On the other hand, the BB

setting may offer utility in cases of the base model internals not being accessible.

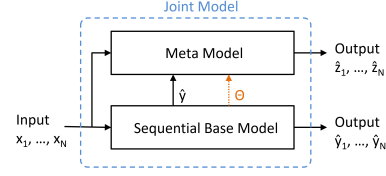


Figure 1. The concept of meta modeling

While the MM concept applies to all tasks including classification, detection, ranking, and regression, this work focuses on the latter exclusively.

We now formalize the MM concept for sequential regression. Let $\hat{\mathbf{y}} = F_\phi(\mathbf{x})$ be the base model function parametrized by ϕ , where $\mathbf{x} = x_1, \dots, x_N$ and $\hat{\mathbf{y}} = \hat{y}_1, \dots, \hat{y}_M$ represent sequences of N input feature vectors and M D -dimensional output vectors, with $\hat{\mathbf{y}} \in \mathbb{R}^{D \times M}$. Let $\hat{\mathbf{z}} = G_\gamma(\hat{\mathbf{y}}, \mathbf{x}, \phi)$ denote the meta model, parameterized by γ , taking as input the predictions, the original features, and the parameters of the base to produce a sequence of error predictions, $\hat{\mathbf{z}} \in \mathbb{R}^{D \times M}$. The parameters ϕ are obtained by solving an optimization problem, $\arg \min_\phi \mathbb{E}[l_b(\hat{\mathbf{y}}, \mathbf{y})]$, using a smooth loss function l_b , e.g., the Frobenius norm $l_b = \|\hat{\mathbf{y}} - \mathbf{y}\|_F^2$. Similarly, the parameters γ are determined via $\arg \min_\gamma \mathbb{E}[l_m(\hat{\mathbf{z}}, \mathbf{z})] = \arg \min_\gamma \mathbb{E}[l_m(\hat{\mathbf{z}}, l_z(\hat{\mathbf{y}}, \mathbf{y}))]$ involving a loss l_z quantifying the target error (residual) from the base model, and l_m quantifying the prediction error of the meta model. In general, l_b , l_z , and l_m , may differ. The expectations are estimated using an available dataset. We used the L_F^2 norm for l_b and l_m , and L_1 for l_z , as described in Section 4.2. Given the loss functions above and the DNN setting, the base and the meta model can be integrated in a single network (JM). In this case the parameters are estimated jointly via

$$\phi^*, \gamma^* = \arg \min_{\phi, \gamma} \mathbb{E}[\beta l_b(\hat{\mathbf{y}}, \mathbf{y}) + (1 - \beta) l_m(\hat{\mathbf{z}}, l_z(\hat{\mathbf{y}}, \mathbf{y}))] \quad (1)$$

whereby dedicated output nodes of the network generate \hat{y}_t and \hat{z}_t , and β is a hyper-parameter trading off the base with the meta loss. Thus, one part of the network tackles the base task, minimizing the base residual, while another models the residual as the eventual measure of uncertainty. As done in (Kendall & Gal, 2017), one can argue that the base objective minimizes the epistemic (parametric) uncertainty, while the meta objective captures the aleatoric uncertainty present in the data. Due to their interaction, the base loss is influenced by the estimated uncertainty encouraging it to focus on feature-space regions with lower aleatoric uncertainty. Moreover, the base model is encouraged to encode the input in ways suitable for uncertainty quantification.

Figure 2 shows an overview of a sequential DNN architecture applied throughout our study. It includes a base encoder-decoder pair and a meta decoder connected to them. Each of these contains a recurrent memory cell - the LSTM (Hochreiter & Schmidhuber, 1997). The role of the encoder is to process the sequential input, \mathbf{x} , to compress its information in a context vector and pass it to the base decoder. The recurrent decoder produces the regression output $\hat{\mathbf{y}}$ in M time steps. Evolving in time, both base LSTMs update their internal states b_t and h_t (see Fig. 2), with the last state, b_N , serving as the starting context in the decoder. The decoder consumes its own prediction from the previous time step as input to generate the next output. This architecture has gained wide popularity in applications such as speech-to-text (Chiu et al., 2018; Tüske et al., 2019), text-to-speech (Sotelo et al., 2017), machine translation (Sutskever et al., 2014), and image captioning (Rennie et al., 2016). Following the MM concept, we attach an additional decoder (the meta decoder) via connections to the encoder and decoder outputs. The context vector, b_N , is transformed by a fully connected layer (FCN in Figure 2), and both the \hat{y}_t output as well as the internal state, h_t , are fed into the meta component. As mentioned above, the meta decoder generates uncertainty estimates, \hat{z}_t .

Given the architecture depicted in Figure 2, we summarize the three settings as follows:

- Joint Model (JM): parameters are trained according to Eq. (1) with certain values of β
- White-Box model (WB): base parameters ϕ are trained first, with $\beta = 1.0$. Then, with ϕ fixed (non-trainable), parameters γ are estimated.
- Black-Box model (BB): the meta decoder part of the model is removed, training ϕ only. Then, a separate encoder-decoder model is trained based solely on the input \mathbf{x} to predict the residual \mathbf{z} .

3.1.1. GENERATING SYMMETRIC AND ASYMMETRIC BOUNDS

The choice of loss function, l_z , gives rise to two scenarios. If l_z is an even function, e.g., $l_z(\hat{\mathbf{y}}, \mathbf{y}) = \|\hat{\mathbf{y}} - \mathbf{y}\|_1$, the predictions $\hat{\mathbf{z}}$ reflect symmetric uncertainty. If, on the other hand, l_z takes the sign in z into account, it is possible to dedicate separate network nodes $\gamma_l, \gamma_u \in \gamma$ to produce lower and upper band¹ estimates, $\hat{\mathbf{z}}_l$ and $\hat{\mathbf{z}}_u$, respectively, thus accomplishing asymmetric prediction. Let $\delta = \hat{\mathbf{y}} - \mathbf{y}$. For the asymmetric scenario the meta objective is modified as follows:

$$\gamma^* = \arg \min_{\gamma} \mathbb{E}[l_m(\mathbf{z}_l, \max\{\delta, 0\}) + l_m(\mathbf{z}_u, \max\{-\delta, 0\})]$$

¹The term “band” refers to the bound’s positive deviate from \hat{y}

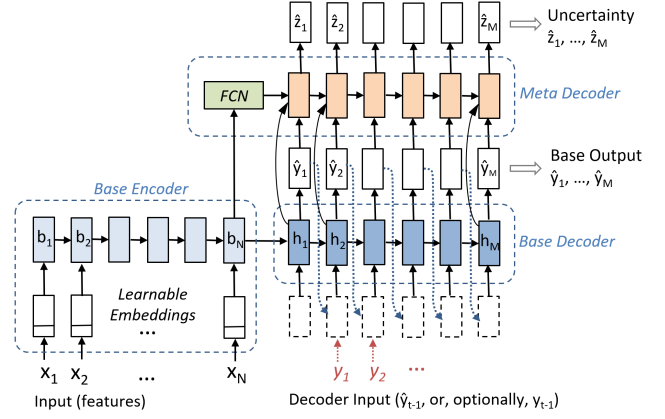


Figure 2. Encoder-Decoder architecture integrating a base and a meta model

(2)

Overall, for a D -dimensional regression output at time t , $y_t \in \mathbb{R}^D$, the meta decoder will have D uncertainty output nodes in the symmetric and $2D$ outputs in the asymmetric case.

3.2. Baselines

3.2.1. IMPLICIT HETEROSKEDASTIC VARIANCE

(Lakshminarayanan et al., 2017; Kendall & Gal, 2017; Oh et al., 2020) applied a Gaussian model $\mathcal{N}(\mu, \sigma^2)$ to the output of a neural network predictor, where μ represents the prediction and σ^2 its uncertainty due to observational (aleatoric) noise. The model is trained to minimize the negative log-likelihood (NLL), with the variance being an implicit uncertainty parameter (in that it is trained indirectly) which is allowed to vary across the feature space (heteroskedasticity). We apply the Gaussian in the sequential setting by planting it onto the base decoder’s output (replacing the meta decoder) and train the network using the NLL objective:

$$\phi^* = \arg \min_{\phi} \mathbb{E} \left[\sum_{t=1}^M \sum_{d=1}^D \frac{(\hat{y}_{t,d} - y_{t,d})^2}{\sigma_{t,d}^2} + \log \sigma_{t,d}^2 \right] \quad (3)$$

with D output nodes modeling the regression variable, \hat{y}_t , and separate D output nodes modeling the $\log \sigma_t^2$, at time t .

This approach resembles the meta-modeling concept somewhat but deviates in that the variance parameter is not supervised using the residual target but emerges as a by-product of the Gaussian model.

3.2.2. VARIATIONAL DROPOUT

(Gal & Ghahramani, 2016) established a connection be-

tween dropout (Srivastava et al., 2014), i.e., the process of randomly omitting network connections, and an approximate Bayesian inference. Their work suggests applying the dropout principle to the inputs, internal states, as well as outputs of the recurrent cells. However, unlike with traditional dropout, the method is applied both in training and test, and for each RNN sequence the dropout pattern is kept fixed.

We apply the variational dropout method to the base encoder and decoder. By performing multiple runs per test sequence, each with a different random dropout pattern, the base predictions are calculated as the mean and the base uncertainty as the variance over such runs.

The Bayesian method, along with the variational approximation, captures the parametric (epistemic) uncertainty of the model, hence it fundamentally differs from the Gaussian model as well as our proposed approach.

3.2.3. GARCH VARIANCE

Introduced in (Bollerslev, 1986; Engle, 1982), the Generalized Autoregressive Conditional Heteroskedastic (GARCH) variance model belongs among the most popular statistical methods. A GARCH(p,q) assumes the series to follow an autoregressive moving average model and estimates the variance at time t as a linear combination of past q residual terms, ϵ^2 , and p previous variances, σ^2 :

$$\sigma_t^2 = \alpha_0 + \sum_{i=1}^q \alpha_i \epsilon_{t-i}^2 + \sum_{i=1}^p \beta_i \sigma_{t-i}^2 \quad (4)$$

The α_0 term represents a constant component of the variance. The parameters, α, β are estimated via maximum-likelihood on a training set. The GARCH process relates to the concept in Figure 1 in that it acts as the meta-model predicting the squared residual. At training time, we take the residual $\epsilon_t = \hat{y}_t - y_t$ using predictions from the base model, while at test time, the residual is approximated using an autoregressive component. We use the GARCH as a baseline only on one of the datasets for reasons discussed in Section 4.2.2.

3.2.4. NAIVE BASELINES

A consistent comparison of uncertainty methods is difficult due to the fact that each generates an uncertainty around different base predictions. Therefore, as a reference we also generate a constant symmetric band around each base predictor. A constant bound represents a homoskedastic process – a sensible choice in many well-behaved sequential regression problems, corresponding to a GARCH(0,0) model. We will use this reference point to compute a relative gain of each method as explained in Section 3.4.

3.3. Evaluation Methodology

3.3.1. CORE METRICS

We propose several metrics to assess the quality of the uncertainty predictions. Unlike with classification tasks, where standard calibration-based metrics apply (Snoek et al., 2019), we need to consider two aspects arising in regression, roughly speaking: (1) what is the extent of observations falling outside the uncertainty bounds (Type 1 cost), and (2) how excessive in width are the bounds (Type 2 cost). An optimal bound captures all of the observation while being least excessive in terms of its bandwidth. (Shen et al., 2018) defined two measures reflecting these aspects (miss rate and bandwidth) and we expand on these. Let $\hat{\mathbf{y}}^l = \hat{\mathbf{y}} - \hat{\mathbf{z}}_l$ and $\hat{\mathbf{y}}^u = \hat{\mathbf{y}} + \hat{\mathbf{z}}_u$ denote the predicted lower and upper band, respectively. Recall that $\hat{\mathbf{y}} \in \mathbb{R}^{D \times M}$. We define the following metrics:

$$\text{Missrate}(\hat{\mathbf{y}}^l, \hat{\mathbf{y}}^u, \mathbf{y}) = 1 - \frac{1}{MD} \sum_{d,t: y_{dt} \in [\hat{y}_{dt}^l, \hat{y}_{dt}^u]} 1 \quad (5)$$

$$\text{Bandwidth}(\hat{\mathbf{y}}^l, \hat{\mathbf{y}}^u, \mathbf{y}) = \frac{1}{2MD} \sum_{d=1}^D \sum_{t=1}^M \hat{y}_{dt}^u - \hat{y}_{dt}^l \quad (6)$$

$$\begin{aligned} \text{Excess}(\hat{\mathbf{y}}^l, \hat{\mathbf{y}}^u, \mathbf{y}) &= \\ &= \frac{1}{MD} \sum_{d,t: y_{dt} \in [\hat{y}_{dt}^l, \hat{y}_{dt}^u]} \min \{y_{dt} - \hat{y}_{dt}^l, \hat{y}_{dt}^u - y_{dt}\} \end{aligned} \quad (7)$$

$$\begin{aligned} \text{Deficit}(\hat{\mathbf{y}}^l, \hat{\mathbf{y}}^u, \mathbf{y}) &= \\ &= \frac{1}{MD} \sum_{d,t: y_{dt} \notin [\hat{y}_{dt}^l, \hat{y}_{dt}^u]} \min \{|y_{dt} - \hat{y}_{dt}^l|, |y_{dt} - \hat{y}_{dt}^u|\} \end{aligned} \quad (8)$$

Figure 3 illustrates these metrics. The relative proportion of observations lying outside the bounds (miss rate) ignores the *extent* of the bound’s short fall. The Deficit, Eq. (8), captures this. The type 2 cost is captured by the Bandwidth, Eq. (6). However, its range is indirectly compounded by the underlying variation in $\hat{\mathbf{y}}$ and \mathbf{y} . Therefore we propose the Excess measure, Eq. (7), which also reflects the Type 2 cost, but just the portion above the minimum bandwidth necessary to include the observation. Note that the above definitions involve uniform averaging over the dimensions. In some cases it may be desirable to use weighted averaging in order to equalize the impact of individual dimensions.

3.3.2. CALIBRATION

In general, DNNs offer few guarantees about the behavior of their output. It is known that DNNs tend to produce miscalibrated classification probabilities (Guo et al., 2017). In

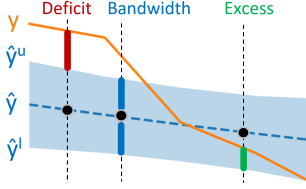


Figure 3. Bandwidth, excess, and deficit costs.

order to evaluate the regression uncertainty across models, it is necessary to establish a common operating point (OP). We achieve this via a scaling calibration. For symmetric bounds, we assume that $\mathbf{y} = \hat{\mathbf{y}} + \hat{\mathbf{z}} \odot \epsilon$ where $\epsilon \in \mathbb{R}^{D \times M}$ is a random i.i.d. matrix and $\hat{\mathbf{z}}$ is the non-negative uncertainty prediction. Let $Z_{dt} = \frac{y_{dt} - \hat{y}_{dt}}{\hat{z}_{dt}}$. Using a held-out dataset, we can obtain an empirical distribution in each output dimension: $\text{cdf}(\{Z_{dt}\}_{1 \leq t \leq M})$, $d = 1, \dots, D$. It is then possible to find the value $\varepsilon_d^{(p)}$ for a desired quantile p , e.g., $\varepsilon_d^{(0.95)}$, and construct the prediction bound at test time: $[\hat{y}_{dt} - \hat{z}_{dt}\varepsilon_d^{(p)}, \hat{y}_{dt} + \hat{z}_{dt}\varepsilon_d^{(p)}]$. Assuming Z_d is stationary, in expectation, this bound will contain the desired proportion p of the observations, i.e., $\mathbb{E}[\text{Missrate}(\hat{\mathbf{y}}^l, \hat{\mathbf{y}}^u, \mathbf{y})] = 1 - p$.

This scaling is applied in our evaluation to compare the excess, bandwidth and deficit at fixed miss rates as well as setting a minimum cost OP (see Section 3.4). An Algorithm to find a scale factor for a desired value of any of the four metrics in $O(M^2)$ operations is given in the Appendix.

3.4. Metrics Used in Reporting

Recall that an OP refers to a value of a desired metric measured at a fixed value of a second metric. The following OP-based measures are used in reporting: (1) Excess, Deficit, Bandwidth at a fixed Missrate, averaged over $\text{Missrate} = \{0.1, 0.05, 0.01\}$, and (2) Minimum Excess-Deficit cost, where $\text{cost} = \frac{1}{2}(\text{Excess} + \text{Deficit})$ with the minimum over all scales.

As alluded to in Section 3.2.4, for each system and measure, m_s , the symmetric constant-band baseline, m_{fixed} , is also created and the relative percent gain with respect to this reference calculated: $\text{gain}_s = 100 \times \frac{m_{fixed} - m_s}{m_{fixed}}\%$. As the main measure for symmetric results we choose the average of Excess and Deficit over the above-listed Missrate range, and the minimum cost. When reporting asymmetric results we also give the Bandwidth average over same Missrate range.

Finally, the error rate of the base predictor is calculated as $E_{base}(\hat{\mathbf{y}}, \mathbf{y}) = \frac{1}{D} \sum_{d=1}^D \frac{\|\hat{y}_d - y_d\|_1}{\|y_d\|_1}$, where \hat{y}_d, y_d are d -th row vectors of $\hat{\mathbf{y}}, \mathbf{y}$.

4. Experiments

4.1. Datasets

Two sequential regression datasets, namely the *Metro Interstate Traffic Volume (MITV)* dataset² and the *SPE9 Reservoir Production Rates (SPE9PR)* dataset³, were experimented with. Both originate from real-world applications, involve sequential input/output variables, and provide for scenarios with varying degrees of difficulty.

4.1.1. METRO INTERSTATE TRAFFIC VOLUME (MITV)

The dataset is a collection of hourly westbound-traffic volume measurements on Interstate 94 reported by the Minnesota DoT ATR station 301 between the years 2012 and 2018. These measurements are aligned with hourly weather features⁴ as well as holiday information, also part of the dataset. The target of regression is the hourly traffic volume. This dataset was released in May, 2019.

The MITV input features were preprocessed to convert all categorical features to trainable vector embeddings, as outlined in Figure 2. All real-valued features as well as the regression output were standardized before modeling (with the test predictions restored to their original range before calculating final metrics). Overall dataset statistics are listed in Table 1, further processing steps are given in Section 4.2, and complete pre-processing details listed in the Appendix.

4.1.2. SPE9 RESERVOIR PRODUCTION RATES (SPE9PR)

This dataset originates from an application of oil reservoir modeling. A reservoir model (RM) is a space-discretized approximation of a geological region subject to modeling. Given a sequence of drilling actions (input), a physics-based PDE-solver (simulator) is applied to the RM to generate sequences of future production rates (oil, gas, water production), typically over long horizons (Killough, 1995). The objective is to train a DNN and accurately predict outputs on unseen input sequences. We used the publicly available SPE9⁵ RM, considered a reference for benchmarking reservoir simulation in the industry, and an open-source simulator⁶ to produce 28,000 simulations, each with 100 randomized actions (varying type, location, and control parameters of a well) inducing production rate sequences over a span of 25 years, in 90-day increments, i.e., 100 time steps.

²<https://archive.ics.uci.edu/ml/machine-learning-databases/00492/>

³<https://developer.ibm.com/exchanges/data/all/oil-reservoir-simulations/>

⁴provided by OpenWeatherMap

⁵<https://github.com/OPM/opm-data/blob/master/spe9/SPE9.DATA>

⁶<https://opm-project.org/>

Table 1. Overview statistics of the MITV and the SPE9PR datasets

Dataset	Total Samples	Input Features	Output Dim	Time Resol.	Partition Size				
					TRAIN	DEV	DEV2	TEST	TEST (drift)
MITV	48204	8	1	1 hr	33744	4820	4820	4820	n/a
SPE9PR	28000 $\times 100$	248	4	90 days	24000 $\times 100$	1000 $\times 100$	1000 $\times 100$	1000 $\times 100$	1000 $\times 100$

Furthermore, the RM was partitioned into two regions, A and B. While most of the actions are located in the region A, we also generated 1000 sequences with actions located in the region B thus creating a large degree of mismatch between training and test. The test condition in region B will be referred to as “drift” scenario.

Basic preprocessing, including standardization and vector embedding of categorical variables was performed, resulting in 268-dimensional input feature vectors. The output variable is a 4-dimensional vector capturing 3 production rates (oil, gas, water) and 1 injection rate (water). Additional detail is given in the Appendix. We are releasing this dataset to the ML community.

4.2. Training Procedure

Each dataset was partitioned into TRAIN, DEV, DEV2, and TEST sets (with SPE9PR also providing a TEST-drift set), as listed Table 1. While the TRAIN/DEV partitions served basic training, the DEV2 was used in determining certain hyperparameters and metric operating points (calibration). The TEST sets were used to produce the reported metrics.

While a single sample in the SPE9PR represents a sequence of 100 steps, the MITV data come as a single contiguous sequence. After partitioning, each MITV sequence was processed by a sliding window of length 36 hours (in 1-hour steps). This resulted in a series of $(n - 35) \times 36$ subsequences (n denotes the partition size) to feed the encoder-decoder model. When testing on the MITV, DNN predictions from such sliding windows were recombined into a contiguous prediction sequence by skipping blocks of windows.

4.2.1. COMMON STEPS

The base encoder-decoder network (see Figure 2) is trained using the Adam optimizer (Kingma & Ba, 2014) with a varying initial learning rate, lr , in two stages:

1. Train all parameters using TRAIN set with $\text{lr}=0.001$. Early stopping determined on the DEV set. The $t-1$ ground truth is used for all decoder inputs at t (see Figure 2).
2. Build on model from previous step, using TRAIN,

$\text{lr}=0.0002$, but switch to using previous decoder output, \hat{y}_{t-1} as input in the current step, referred to as *emulation* (Bengio et al., 2015). Only for the MITV setup: Continue using the ground truth for the first 12 time steps before switching to emulation mode for the rest 24 steps, thus considering the 12 hours as an observed period for every 24-hour prediction period.

All other hyperparameter values are listed in detail in the Appendix. Their values originate from a separate study related to the SPE9 reservoir modeling (Navrátil et al., 2019).

4.2.2. INDIVIDUAL SYSTEMS

Joint Model, Symmetric (JMS), and Asymmetric (JMA): The common training steps are performed using the objective in Eq. (1), with $\beta = 1.0$, first. Then, the joint training continues with $\beta = 0.5$ as long as the objective improves on DEV. In a final step, the model switches to using DEV as training with $\beta = 0.0$ until no improvement on TRAIN is seen. This step helps the meta model see patterns from the base outside its training set. A similar procedure is followed for the JMA, except using Eq. (2).

White-Box Model, Symmetric (WBMS): The basic training is performed with $\beta = 1.0$. Next, only meta model parameters are estimated using the DEV/TRAIN sets with $\beta = 0.0$.

Black-Box Model, Symmetric (BBMS): Base training is performed. The base model processes the DEV set to generate residual \mathbf{z} . A separate encoder-decoder model is then trained using (\mathbf{x}, \mathbf{z}) .

Joint Model with Variance (JMV): The two common steps are performed using the NLL objective (Eq.3) with the variance-related parameters first fixed, and, in a subsequent step, allowing the variance parameters to be adjusted, until convergence. This is to aid stability in training (Nix & Weigend, 1994).

Dropout Model Symmetric (DOMS): Dropout with a rate of 0.25 (inputs, outputs) and 0.1 (internal states), determined as best performing on the DEV2 set, were applied in both the base encoder and the decoder. The two common steps were performed. At test time, the model was run 10 times per each test sequence to obtain the mean prediction

and standard deviation.

GARCH: The GARCH model from Section 3.2.3 is used with $p = q = 5$. The lag value was determined using an autocorrelation chart showing attenuation at lags > 5 . We only apply this baseline to the MITV dataset as it provides a contiguous time series. The model parameters were trained using the DEV2 partition.

Throughout the experiments, the size of each LSTM cell was kept fixed at 32 for the base encoder/decoder, and at 16 for the meta decoder. The base sizing has been largely driven by our preliminary study showing it suffices in providing accurate base predictions.

4.3. Testing Procedure

With the MITV dataset, we want to simulate a scenario in which given the past 12 hours worth of traffic observations the model is to make a forecast for the next 24 hours. This is achieved by spanning a 36-hour window and giving the decoder access to the first 12 hours of ground truth (see Step 2 in Section 4.2.1). Note that when recombining the windowed predictions, only the net-forecast 24-hour segments are taken. Furthermore, in order to gauge the model behavior in a mismatched scenario, we add testing the MITV models without providing those first 12 hours of observation. Loosely speaking, this emulates a “drift” condition as the model was trained to rely on the ground truth information but now receives estimates of the same only.

No special post-processing is necessary on the SPE9PR predictions, the metrics are averaged over all simulations, timesteps, and output dimensions.

4.4. Results with Symmetric Bounds

Table 2 compares the proposed symmetric-bounds systems (JMS, WBMS, BBMS) with the baselines (JMV, DOMS, GARCH). The relative error of the base predictor is given in the E_{base} column. The uncertainty quality is reported in Table 2 is the average gain in excess-deficit metrics, as defined in Section 3.4. Columns labeled as G^* contain measurements made at an operating point (OP) determined on the test set itself, while those labeled as G^{xval} use an OP from a held-out (DEV2) set. While G^{xval} reflects generalization of the calibration, G^* values are interesting as they reveal the potential of each method. Based on a paired permutation test (Dwass, 1957), all but entries marked with † are mutually significant at $p < 0.01$.

From Table 2 we make the following observations: (1) the JMS model dominates all other models across all conditions. The fact that it outperforms the WBMS indicates there is a benefit to the joint training setup, as conjectured earlier. (2) The WBMS dramatically outperforms the BBMS model, which remains only as good as a constant band for MITV

data. It appears it is hard to reliably predict residuals from only the input features. (3) The most competitive baseline is the JMV model. As discussed in Section 3.2.1, the JMV shares some similarity with the meta-modeling approach. (4) The JMS and WBMS models perform particularly well in the strong drift scenario (SPE9PR), suggesting that white-box features play an essential role in achieving generalization. Finally, (5) the DOMS model works moderately well on MITV data but provides no benefit in the SPE9PR, which could be due the aleatoric uncertainty playing a dominant role in this dataset. In almost all cases, however, the averaging of base predictions in DOMS results in lowest error rates of the base predictor.

Representative samples of JMS and JMV uncertainty bounds are shown in Figure 4 (MITV) and Figure 5 (SPE9PR). They illustrate a clear trend in the results, namely that the JMS (also seen with WBMS) model are better able to cover the actual observation, particularly when the base prediction tends to make large errors.

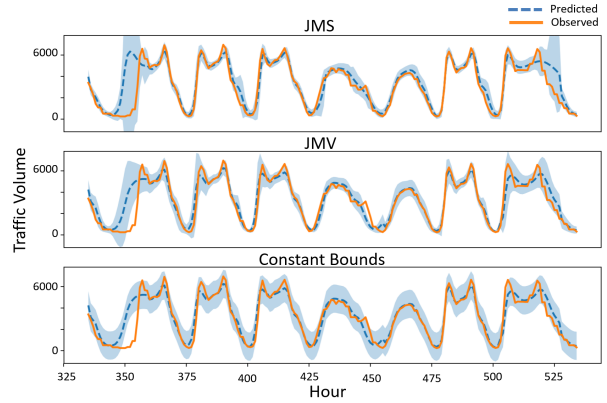


Figure 4. Sample of traffic volume predictions with uncertainty generated by the JMS and JMV models, along with a constant band (around JMV) (miss rate set to 0.1 on TEST).

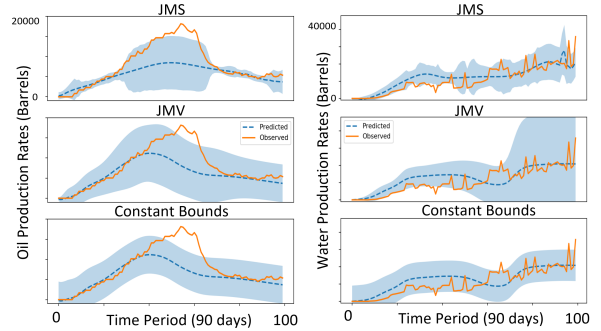


Figure 5. SPE9PR samples of oil (left) and water (right) production rates (“drift” scenario, miss rate set to 0.1 on TEST).

Table 2. Relative optimum and cross-validated gains (G^* , G^{xval}) using the Excess-Deficit metrics. E_{base} denotes the base predictor’s error. Within each column, elements marked[†] are in a statistical tie, all other values are mutually significant at $p < 0.01$

System	MITV						SPE9PR					
	match			drift			match			drift		
	E_{base}	% G^*	% G^{xval}	E_{base}	% G^*	% G^{xval}	E_{base}	% G^*	% G^{xval}	E_{base}	% G^*	% G^{xval}
JMS	.155 [†]	57.8[†]	59.3[†]	.187 [†]	52.5	55.6	.165	46.5	46.6	.291	56.6	50.5
WBMS	.159 [†]	53.8[†]	55.3[†]	.190 [†]	39.4	42.3	.162	44.8	44.9	.313	54.5	43.8
JMV	.167	20.4	25.5	.179	20.0 [†]	17.5 [†]	.159	45.3	45.5	.334	-6.5	4.4
DOMS	.144	13.2	12.8	.155	16.6 [†]	17.3 [†]	.177	1.3	1.4	.279	-0.2	-5.2
BBMS	.153 [†]	-0.4	1.2	.188 [†]	-8.9	-3.0	.170	31.9	30.3	.326	11.6	12.8
GARCH	.155 [†]	-1.8	3.1	.187 [†]	-14.7	-4.0	n/a	n/a	n/a	n/a	n/a	n/a

Table 3. Relative gains on Bandwidth and Excess-Deficit metrics for the asymmetric JMA model.

Evaluation	MITV		SPE9PR	
	match	drift	match	drift
JMA Base Error	.158	.200	.168	.320
Bandwidth	JMA, opt. % gain	44.1	37.0	35.5
	JMA, xval % gain	33.1	26.4	35.5
	JMS, opt. % gain	37.5	31.6	29.1
	JMS, xval % gain	35.2	27.2	28.7
Ex-Deficit	JMA, opt. % gain	45.3	29.0	30.9
	JMA, xval % gain	40.4	28.6	30.8
	JMS, opt. % gain	57.8	52.5	46.5
	JMS, xval % gain	59.3	55.6	46.6

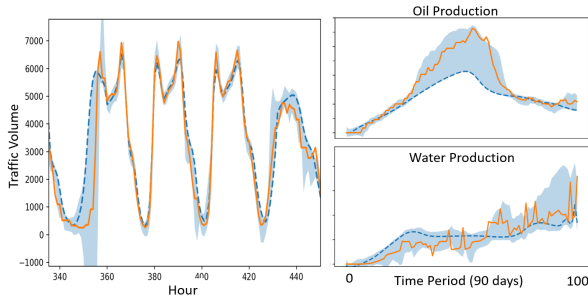


Figure 6. Samples of asymmetric bounds produced by the JMA. MITV sample (left) and SPE9PR (right) correspond to segments shown in Figure 4 and 5.

4.5. Results with Asymmetric Bounds

Generating asymmetric bounds is a new intriguing aspect of DNN-based meta-models. Using the JMA model, we first recorded the accuracy with which the asymmetric output agrees *in sign* (orientation) with the observed base discrepancy. Averaged over the two datasets, this accuracy is at 83.3%, and 91.1% when filtering out samples with small deviations from the ground truth (noise). The promise of asymmetric bounds lies in its potential to reduce the *band-*

width cost. Since the Excess and Deficit metrics ignore the absolute bandwidth, we also evaluate the JMA model using the Bandwidth metric (Eq. (6)), averaged over the same operating points, as shown in Table 3. The table compares the JMA model to the best symmetric model, JMS. The JMS model outperforms JMA in all scenarios on Excess-Deficit, however, compared on the bandwidth metric, the JMA dominates its JMS counterpart benefiting from its orientation capability. The JMA model may be at disadvantage in cases where it produces an incorrect orientation causing excessively large bounds in the incorrect direction due to scaling. A lower- and upper-bound-specific calibration might mitigate this problem. Upon visual inspection, the output of the JMA is appreciably better in bandwidth: Figure 6 shows samples on both datasets. In most instances the bounds behave as one would expect, expending the bulk of the bandwidth in the correct direction. An interesting question arises whether it is possible to utilize the asymmetric output as a correction on the base predictor. Our preliminary investigation shows that a naive combination leads to degradation in the base error, however, this question remains of interest for future work.

5. Conclusions

In this work we demonstrated that meta-modeling (MM) provides a powerful new framework for uncertainty prediction. Through a systematic evaluation of the proposed MM variants we report considerable relative gains over a constant reference baseline and show that they not only outperform all competitive baselines but also show stability across drift scenarios. A jointly trained model integrating the base with a meta component fares best, followed by a white-box setup, indicating that trainable white-box features play an essential role in the task. Besides symmetric uncertainty, we also investigated generating asymmetric bounds using dedicated network nodes and showed their benefit in reducing the uncertainty bandwidth. We believe these results open an exciting new research avenue for uncertainty quantification in sequential regression.

References

- Arnold, M., Bellamy, R. K. E., Hind, M., Houde, S., Mehta, S., Mojsilović, A., Nair, R., Ramamurthy, K. N., Olteanu, A., Piorkowski, D., Reimer, D., Richards, J., Tsay, J., and Varshney, K. R. Factsheets: Increasing trust in ai services through supplier's declarations of conformity. *IBM Journal of Research and Development*, 63(4/5):6:1–6:13, July 2019. ISSN 0018-8646. doi: 10.1147/JRD.2019.2942288.
- Begoli, E., Bhattacharya, T., and Kusnezov, D. The need for uncertainty quantification in machine-assisted medical decision making. *Nature Mach Intell*, 1:20–23, 2019.
- Bengio, S., Vinyals, O., Jaitly, N., and Shazeer, N. Scheduled sampling for sequence prediction with recurrent neural networks. In *Proceedings of the 28th International Conference on Neural Information Processing Systems - Volume 1*, NIPS15, pp. 11711179, Cambridge, MA, USA, 2015. MIT Press.
- Bollerslev, T. Generalized autoregressive conditional heteroskedasticity. *Journal of Econometrics*, 31(3):307–327, April 1986.
- Chen, J. and Politis, D. N. Optimal multi-step-ahead prediction of arch/garch models and novas transformation. *Econometrics*, 7(3):34, Aug 2019. ISSN 2225-1146. doi: 10.3390/econometrics7030034.
- Chen, T., Navrátil, J., Iyengar, V., and Shanmugam, K. Confidence scoring using whitebox meta-models with linear classifier probes. In *The 22nd International Conference on Artificial Intelligence and Statistics, AISTATS 2019, 16-18 April 2019, Naha, Okinawa, Japan*, pp. 1467–1475, 2019.
- Chiu, C., Sainath, T. N., Wu, Y., Prabhavalkar, R., Nguyen, P., Chen, Z., Kannan, A., Weiss, R. J., Rao, K., Gonnina, E., Jaitly, N., Li, B., Chorowski, J., and Bacchiani, M. State-of-the-art speech recognition with sequence-to-sequence models. In *2018 IEEE International Conference on Acoustics, Speech and Signal Processing (ICASSP)*, pp. 4774–4778, April 2018.
- Dwass, M. Modified randomization tests for nonparametric hypotheses. *Ann. Math. Statist.*, 28(1):181–187, 03 1957. doi: 10.1214/aoms/1177707045.
- Engle, R. F. Autoregressive conditional heteroscedasticity with estimates of the variance of united kingdom inflation. *Econometrica*, 50(4):987–1007, 1982. ISSN 00129682, 14680262.
- Finn, C., Rajeswaran, A., Kakade, S., and Levine, S. Online meta-learning. In Chaudhuri, K. and Salakhutdinov, R. (eds.), *Proceedings of the 36th International Conference on Machine Learning*, volume 97 of *Proceedings of Machine Learning Research*, pp. 1920–1930, Long Beach, California, USA, 09–15 Jun 2019. PMLR.
- Gal, Y. and Ghahramani, Z. A theoretically grounded application of dropout in recurrent neural networks. In Lee, D. D., Sugiyama, M., Luxburg, U. V., Guyon, I., and Garnett, R. (eds.), *Advances in Neural Information Processing Systems 29*, pp. 1019–1027. Curran Associates, Inc., 2016.
- Guo, C., Pleiss, G., Sun, Y., and Weinberger, K. Q. On calibration of modern neural networks. In *Proceedings of the 34th International Conference on Machine Learning - Volume 70*, ICML17, pp. 13211330. JMLR.org, 2017.
- Hochreiter, S. and Schmidhuber, J. Long short-term memory. *Neural Comput.*, 9(8):17351780, November 1997. ISSN 0899-7667. doi: 10.1162/neco.1997.9.8.1735.
- Jiang, H., Kim, B., Guan, M., and Gupta, M. To trust or not to trust a classifier. In Bengio, S., Wallach, H., Larochelle, H., Grauman, K., Cesa-Bianchi, N., and Garnett, R. (eds.), *Advances in Neural Information Processing Systems 31*, pp. 5541–5552. Curran Associates, Inc., 2018.
- Kendall, A. and Gal, Y. What uncertainties do we need in bayesian deep learning for computer vision? In Guyon, I., Luxburg, U. V., Bengio, S., Wallach, H., Fergus, R., Vishwanathan, S., and Garnett, R. (eds.), *Advances in Neural Information Processing Systems 30*, pp. 5574–5584. Curran Associates, Inc., 2017.
- Killough, J. Ninth SPE comparative solution project: A reexamination of black-oil simulation. In *SPE Reservoir Simulation Symposium*. Society of Petroleum Engineers, 1995. doi: 10.2118/29110-ms.
- Kingma, D. P. and Ba, J. Adam: A method for stochastic optimization, 2014. cite arxiv:1412.6980Comment: Published as a conference paper at the 3rd International Conference for Learning Representations, San Diego, 2015.
- Lakshminarayanan, B., Pritzel, A., and Blundell, C. Simple and scalable predictive uncertainty estimation using deep ensembles. In Guyon, I., Luxburg, U. V., Bengio, S., Wallach, H., Fergus, R., Vishwanathan, S., and Garnett, R. (eds.), *Advances in Neural Information Processing Systems 30*, pp. 6402–6413. Curran Associates, Inc., 2017.
- Madry, A., Makelov, A., Schmidt, L., Tsipras, D., and Vladu, A. Towards deep learning models resistant to adversarial attacks. *ArXiv*, abs/1706.06083, 2017.
- Mills, T. C. *Time Series Techniques for Economists*. Number 9780521405744 in Cambridge Books. Cambridge University Press, 1991.

- Navrátil, J., King, A., Rios, J., Kollias, G., Torrado, R., and Codas, A. Accelerating physics-based simulations using end-to-end neural network proxies: An application in oil reservoir modeling. *Frontiers in Big Data*, 2: 33, 2019. ISSN 2624-909X. doi: 10.3389/fdata.2019.00033. URL <https://www.frontiersin.org/article/10.3389/fdata.2019.00033>.
- Nix, D. A. and Weigend, A. S. Estimating the mean and variance of the target probability distribution. In *Proceedings of 1994 IEEE International Conference on Neural Networks (ICNN'94)*, volume 1, pp. 55–60 vol.1, June 1994. doi: 10.1109/ICNN.1994.374138.
- Oh, M., Olsen, P. A., and Ramamurthy, K. N. Crowd counting with decomposed uncertainty. In *AAAI Conference on Artificial Intelligence*, 2020.
- Papoulis, A. and Saunders, H. Probability, Random Variables and Stochastic Processes (2nd Edition). *Journal of Vibration, Acoustics, Stress, and Reliability in Design*, 111(1):123–125, 01 1989. ISSN 0739-3717. doi: 10.1115/1.3269815.
- Rennie, S. J., Marcheret, E., Mroueh, Y., Ross, J., and Goel, V. Self-critical sequence training for image captioning. *CoRR*, abs/1612.00563, 2016.
- Schmidhuber, J. Evolutionary principles in self-referential learning. on learning now to learn: The meta-meta-meta...-hook. Diploma thesis, Technische Universität München, Germany, 14 May 1987. URL <http://www.idsia.ch/~juergen/diploma.html>.
- Shen, Y., Wang, X., and Chen, J. Wind power forecasting using multi-objective evolutionary algorithms for wavelet neural network-optimized prediction intervals. *Applied Sciences*, 8(2):185, Jan 2018. ISSN 2076-3417. doi: 10.3390/app8020185.
- Snoek, J., Ovadia, Y., Fertig, E., Lakshminarayanan, B., Nowozin, S., Sculley, D., Dillon, J., Ren, J., and Nado, Z. Can you trust your model’s uncertainty? evaluating predictive uncertainty under dataset shift. In *Advances in Neural Information Processing Systems*, pp. 13969–13980, 2019.
- Sotelo, J., Mehri, S., Kumar, K., Santos, J. F., Kastner, K., Courville, A. C., and Bengio, Y. Char2wav: End-to-end speech synthesis. In *5th International Conference on Learning Representations, ICLR 2017, Toulon, France, April 24-26, 2017, Workshop Track Proceedings*, 2017.
- Srivastava, N., Hinton, G., Krizhevsky, A., Sutskever, I., and Salakhutdinov, R. Dropout: A simple way to prevent neural networks from overfitting. *Journal of Machine Learning Research*, 15:1929–1958, 2014.
- Starica, C., Herzel, S., and Nord, T. Why does the GARCH(1,1) model fail to provide sensible longer-horizon volatility forecasts? *Econometrics 0508003*, University Library of Munich, Germany, August 2005.
- Sutskever, I., Vinyals, O., and Le, Q. V. Sequence to sequence learning with neural networks. In *Proceedings of the 27th International Conference on Neural Information Processing Systems - Volume 2, NIPS14*, pp. 31043112, Cambridge, MA, USA, 2014. MIT Press.
- Tüske, Z., Audhkhasi, K., and Saon, G. Advancing sequence-to-sequence based speech recognition. *Proc. Interspeech 2019*, pp. 3780–3784, 2019.

Supplementary Material: Uncertainty Prediction for Deep Sequential Regression Using Meta Models

Algorithm 1 Find best scale for a given metric value

Input: Observation, base and meta predictions $\{\hat{y}_t, y_t, \hat{z}_t^l, \hat{z}_t^u\}_{1 \leq t \leq M}$; metric function f ; target value ρ^*
Output: Scale factor ε^*

```

for  $t \leftarrow 1$  to  $M$  do
   $\delta_t \leftarrow \hat{y}_t - y_t$ .
   $\varepsilon_t \leftarrow \begin{cases} \frac{\delta_t}{\hat{z}_t^l} & \text{for } \delta_t \geq 0 \\ -\frac{\delta_t}{\hat{z}_t^u} & \text{otherwise} \end{cases}$ 
  for  $k \leftarrow 1$  to  $M$  do
     $\hat{y}_k^l \leftarrow \hat{y}_k - \varepsilon_t \hat{z}_k^l$ 
     $\hat{y}_k^u \leftarrow \hat{y}_k - \varepsilon_t \hat{z}_k^u$ 
  end for
   $\rho_t \leftarrow f(\{\hat{y}_k^l, \hat{y}_k^u, y_k\}_{1 \leq k \leq M})$ 
end for
 $t^* \leftarrow \arg \min_t |\rho_t - \rho^*|$ 
 $\varepsilon^* \leftarrow \varepsilon_{t^*}$ 

```

A. Algorithm to Find a Scaling Factor

Section 3.3.2 discusses the scaling calibration in the context of the four metrics: Missrate, Bandwidth, Excess, and Deficit. Algorithm 1 finds a scale factor for a desired value of any of these four metrics in $O(M^2)$ operations.

B. Additional Implementation Details

B.1. MITV PreProcessing

As described in Section 4.1.1 and Table 1, the MITV dataset comes with 8 input features, among which 3 are categorical. Here we list the relevant parsing and encoding steps used in our setup. The raw time stamp information was parsed to extract additional features such as day of the week, day of the month, year-day fraction, etc. Table 4 shows the corresponding list. Standardization was performed on the input as well as output, as per Table 4, whereby the model predictions were transformed to their original range before calculating final metrics.

B.2. SPE9PR PreProcessing

The Table 5 lists details on the SPE9PR features (also refer to Section 4.1.2 and Table 1). The SPE9PR dataset contains input sequences of actions and output sequences of production rates. An action (feature `type_of_well`), at a

particular time, represents a decision whether to drill, and if so, what type of well to drill (an injector or a producer well), or not to drill (encoded by "0"), hence the cardinality is 3. In case of a drill decision, further specifications apply, namely the x- and y-location on the surface of the reservoir, local geological features at the site, and well control parameters. There are 15 vertical cells in the SPE9 each coming with 3 geological features (rel. permeability, rel. porosity, rock type), thus the local geology is a 45-dimensional feature vector at a particular (x, y) location. Finally, every well drilled so far may be controlled by a parameter called "Bottom-Hole Pressure" (BHP). Since we provision up to 100 wells of each of the two types, a 200-dimensional vector arises containing BHP values for these wells at any given time. Standardization was performed on the input as well as output as specified in Table 5 whereby the model predictions were transformed to their original range before calculating and reporting final metrics.

B.3. Training Setup

B.3.1. HYPERPARAMETERS

Hyperparameters have been determined in two ways: (1) learning rate, regularization, batch, and LSTM size were adopted from an unrelated experimental study performed on a modified reservoir SPE9 (Anonymized), (2) We used DEV2 to determine the dropout rates in the DOMS model. The value $\beta = 0.5$ was chosen ad-hoc (as a midpoint between pure base and pure meta loss) without further optimization.

B.4. Implementation Notes

All DNNs were implemented in Tensorflow 1.11. Training was done on a Tesla K80 GPU, with total training time ranging between 3 (MITV) and 24 (SPE9PR) hours. The GARCH Python implementation provided in the `arch` library was used.

C. Additional Results

C.1. Individual Metrics

For a more detailed view of the averages in Table 2, we show a split by the individual metrics in Table 7, and, for the SPE9PR which has a total of four output variables, a split by the individual variables in Table 8.

Table 4. MITV Input and Output Specifications

Feature Name	Range	Categorical	Embedding Dimension	Standardized	Final Dimension
INPUT					
day_of_month	integer $\in [0, 30]$	Y	3	N	3
day_of_week	integer $\in [0, 6]$	Y	3	N	3
month	integer $\in [0, 11]$	Y	3	N	3
frac_yday	real $\in [\frac{1}{365}, 1]$	N	-	Y	1
weather_type	integer $\in [0, 10]$	Y	3	N	3
holiday_type	integer $\in [0, 11]$	Y	3	N	3
temperature	real $\in \mathbb{R}$	N	-	Y	1
rain_1h	real $\in \mathbb{R}_0^+$	N	-	Y	1
snow_1h	real $\in \mathbb{R}_0^+$	N	-	Y	1
clouds_all	real $\in [0, 100]$	N	-	Y	1
Total					20
OUTPUT					
traffic_volume	real $\in \mathbb{R}_0^+$	N	-	Y	1
Total					1

C.2. Additional Visualizations

In addition to the sample visualizations shown in Section 2 for the JMS, JMV, and JMA systems, here we show some sections of the data and visualize output of all systems. Figures 7 and 8 show the first simulation in the test set of the SPE9PR dataset for the drift and non-drift condition and all its output components, respectively. Figures 9 and 10 show the output on the MITV drift and non-drift condition, respectively. For each model, a miss rate value of 0.1 across the entire test set was used in the visualizations.

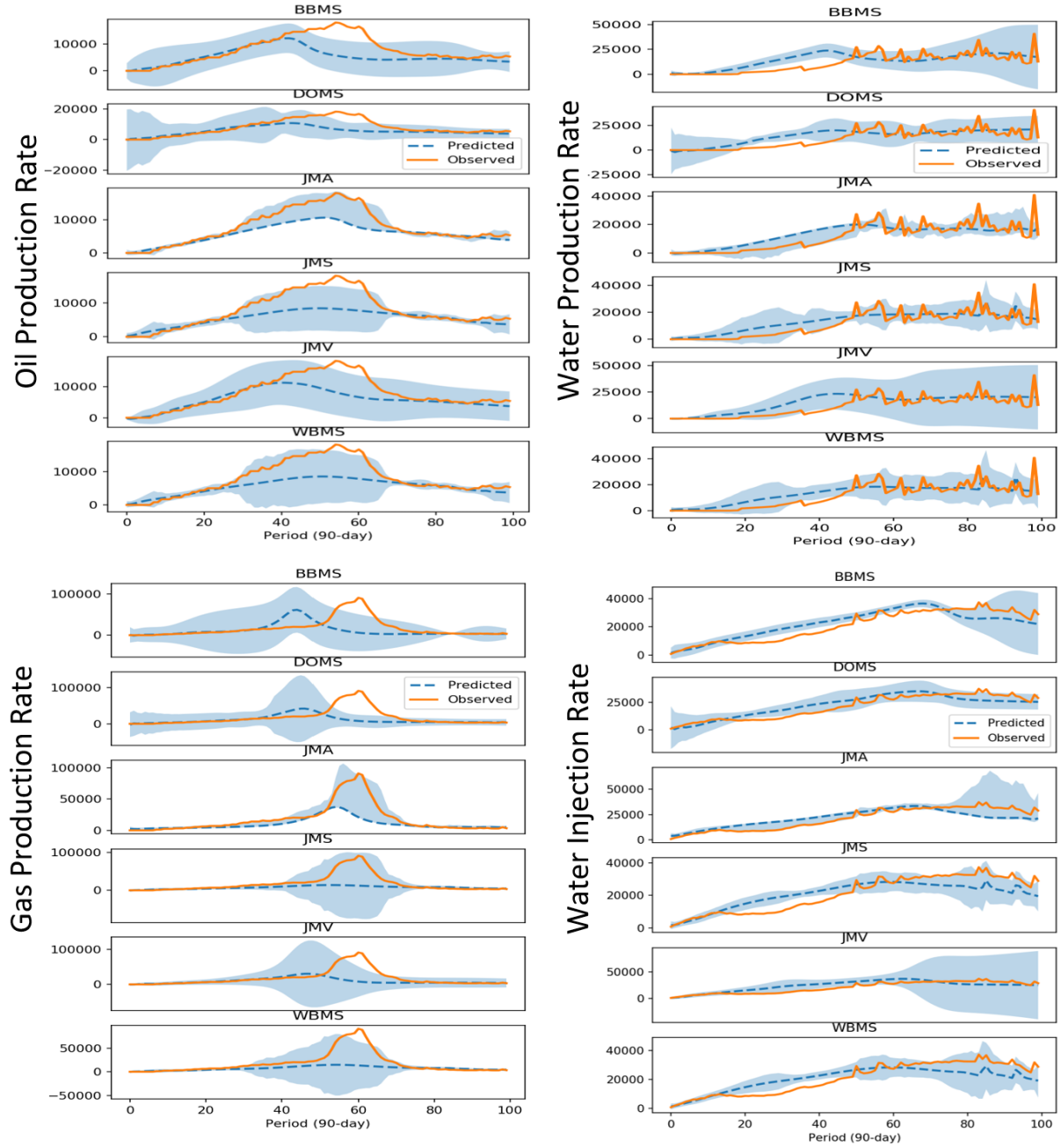


Figure 7. Sample from SPE9PR (simulation 0, drift condition), all components and systems shown.

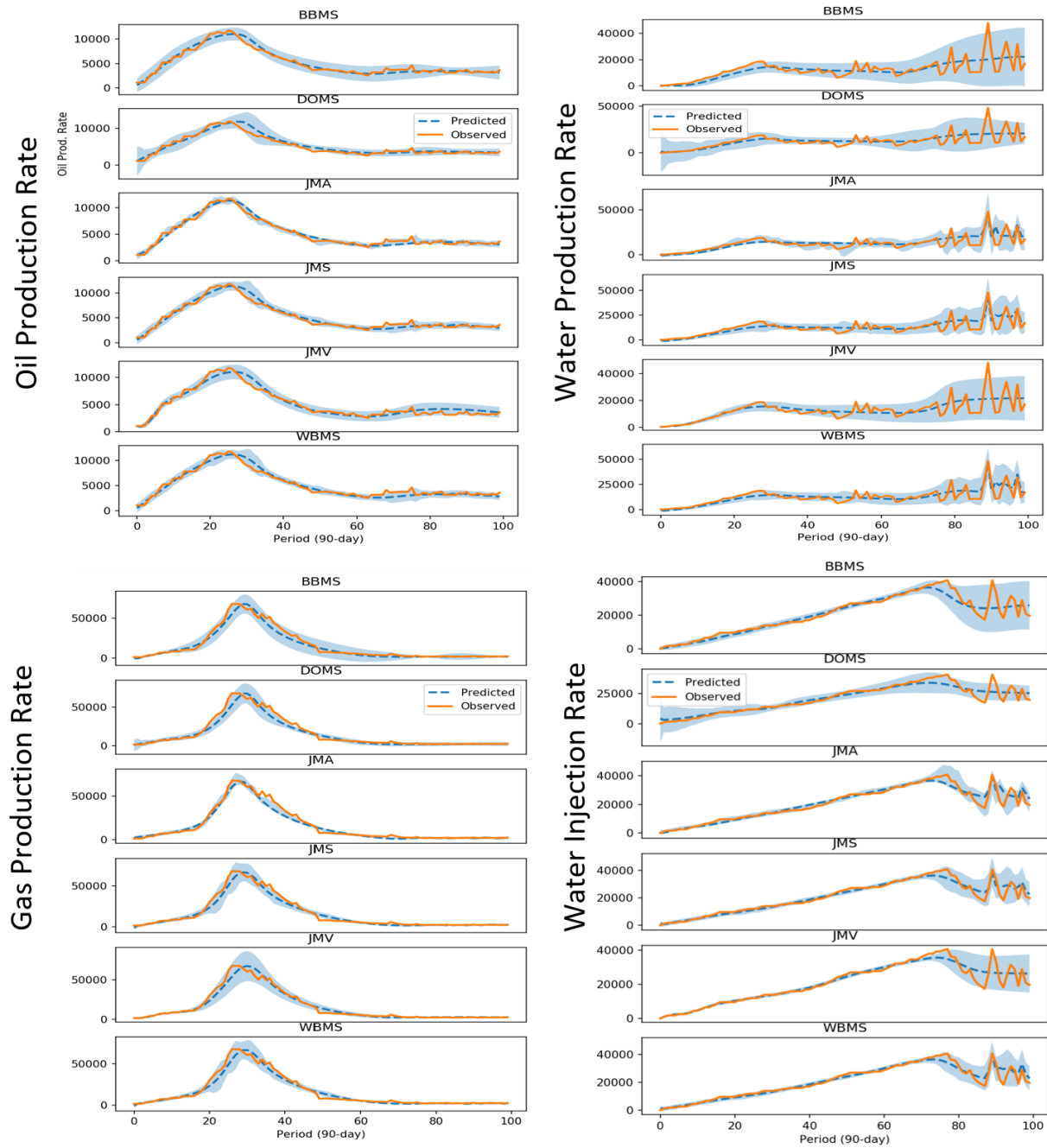


Figure 8. Sample from SPE9PR (simulation 0, non-drift condition), all components and all systems shown.

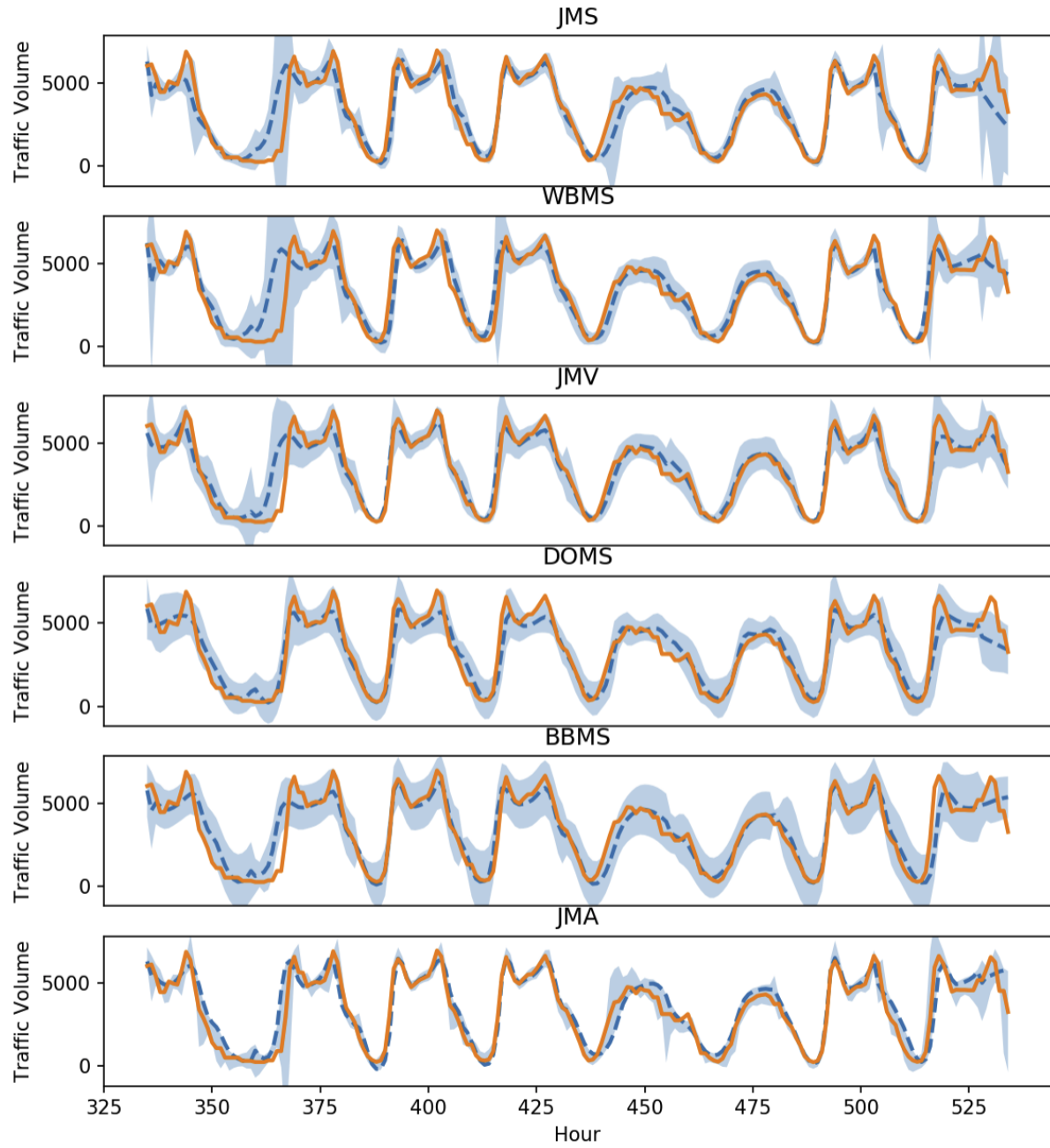


Figure 9. Sample from MITV (drift condition), all systems shown.

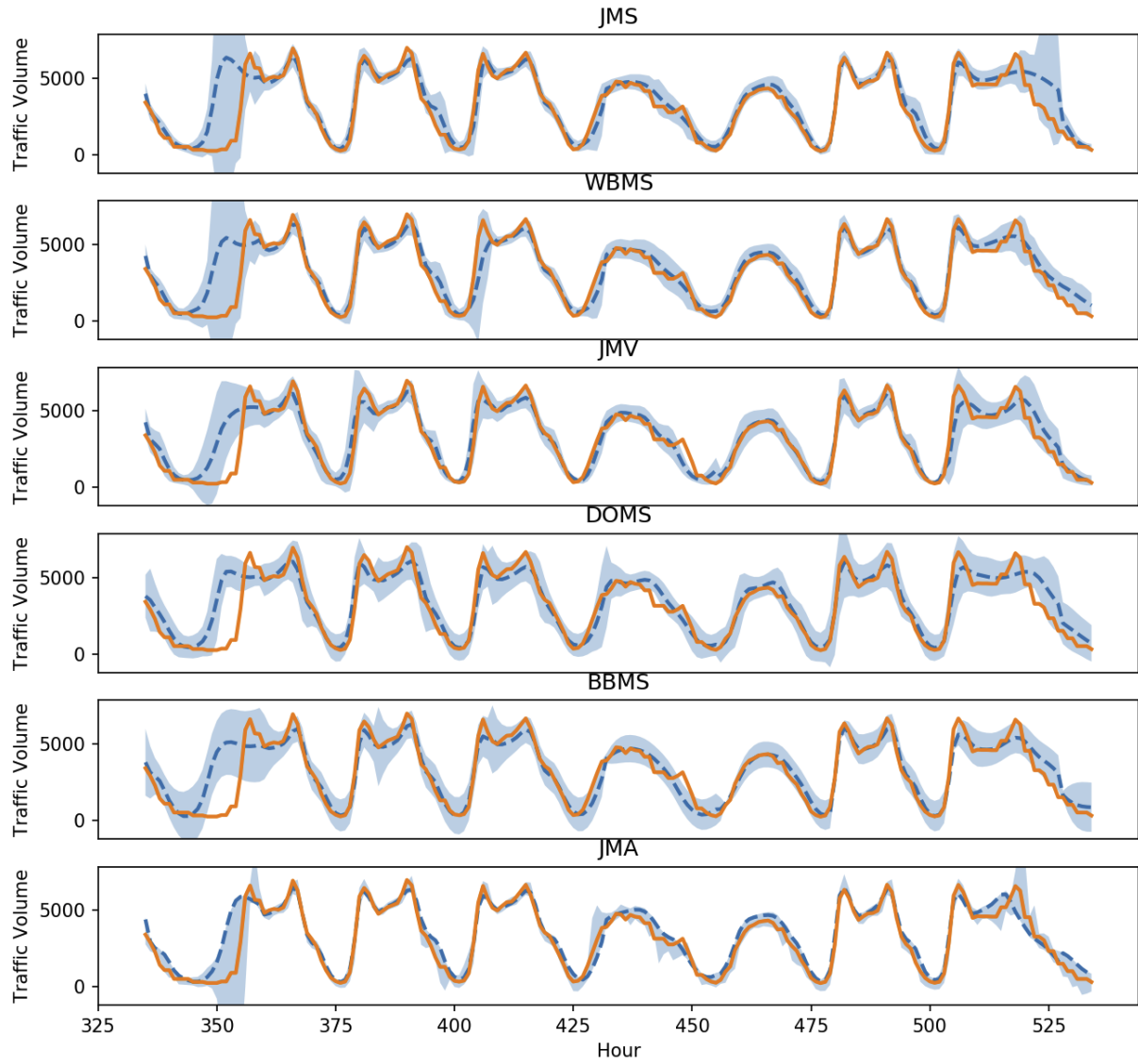


Figure 10. Sample from MITV (non-drift condition), all systems shown.

Table 5. SPE9PR Input and Output Specifications

Feature Name	Range	Categorical	Embedding Dimension	Standardized	Final Dimension
INPUT					
type_of_well	integer $\in \{0, 1, 2\}$	Y	3	N	3
location_x	integer $\in [0, 24]$	Y	10	N	10
location_y	integer $\in [0, 25]$	Y	10	N	10
vertical_geology	real $\in \mathbb{R}^{45}$	N	-	Y	45
per_well_control	real $\in \mathbb{R}^{200}$	N	-	Y	200
Total					258
OUTPUT					
oil_prod_field_rate	real $\in \mathbb{R}_0^+$	N	-	Y	1
gas_prod_field_rate	real $\in \mathbb{R}_0^+$	N	-	Y	1
water_prod_field_rate	real $\in \mathbb{R}_0^+$	N	-	Y	1
water_inj_field_rate	real $\in \mathbb{R}_0^+$	N	-	Y	1
Total					4

Table 6. Hyperparameter settings

Hyper-parameter	Where used	Value	Comment
Learning rate	all	0.001	Stage 1 training
Learning rate	all	0.0002	Stage 2 training, see Section 4.2.1
Batch size	all	100	
L_2 penalty coefficient	all, except DOMS	0.0001	
L_2 penalty coefficient	DOMS	0.0	
Dropout	DOMS	0.25/0.1/0.25	LSTM Input/State/Output (encoder and decoder)
Base LSTM size	all	32	
Meta LSTM size	meta models	16	
β in Eq. (1)	1.0/0.5/0.0	see Section 4.2.2	

Uncertainty in Deep Sequential Regression

Table 7. Symmetric gains split by individual metric (compare to Table 2)

Model	Deficit@0.01	Deficit@0.05	Deficit@0.1	Excess@0.01	Excess@0.05	Excess@0.1	MinCost	Average
%G*, MITV "Non-Drift" Scenario								
JMS	61.3	74.8	75.6	64.5	54.6	40.1	33.9	57.8
WBMS	48.0	73.8	74.3	62.7	50.7	35.1	32.3	53.8
JMV	-33.9	31.9	32.5	35.8	31.4	28.2	16.8	20.4
DOMS	28.1	24.8	23.1	11.5	3.3	-1.6	2.8	13.1
BBMS	9.7	27.9	16.3	-18.8	-18.7	-18.7	-0.8	-0.4
%G ^{xval} , MITV "Non-Drift" Scenario								
JMS	75.9	78.1	77.4	58.0	51.9	39.6	33.9	59.3
WBMS	67.4	79.6	77.7	57.7	42.7	29.8	32.3	55.3
JMV	4.4	38.9	35.8	29.1	27.1	26.3	16.8	25.5
DOMS	78.2	63.9	62.3	-35.7	-32.4	-49.2	2.8	12.8
BBMS	61.6	21.5	15.4	-61.0	-12.5	-15.9	-0.9	1.2
%G*, MITV "Drift" Scenario								
JMS	40.5	78.0	77.5	57.7	45.0	31.9	36.7	52.5
WBMS	18.4	68.8	70.8	43.6	32.8	15.6	25.8	39.4
JMV	-3.8	29.0	30.9	23.0	25.5	21.6	13.8	20.0
DOMS	23.4	23.7	24.7	11.6	14.2	11.4	7.3	16.6
BBMS	-38.2	5.7	8.7	-11.8	-12.2	-14.1	-0.2	-8.9
%G ^{xval} , MITV "Drift" Scenario								
JMS	71.7	81.6	80.1	53.2	39.1	27.1	36.7	55.6
WBMS	67.9	79.2	78.5	22.9	19.4	2.0	25.8	42.3
JMV	-27.2	28.5	32.7	29.1	25.9	19.6	13.8	17.5
DOMS	38.4	18.9	23.4	2.8	16.6	13.3	7.4	17.3
BBMS	6.2	13.2	13.1	-17.5	-17.4	-18.6	-0.3	-3.0
%G*, SPE9PR "Non-Drift" Scenario								
JMS	55.7	55.8	56.8	46.1	42.5	37.7	30.8	46.5
WBMS	50.9	54.5	55.6	47.4	41.5	35.4	28.5	44.8
JMV	50.5	54.2	53.7	51.8	43.3	37.0	26.4	45.3
DOMS	7.1	10.2	10.4	-6.9	-5.8	-6.8	1.0	1.3
BBMS	51.0	52.6	50.0	25.1	18.2	10.6	15.7	31.9
%G ^{xval} , SPE9PR "Non-Drift" Scenario								
JMS	56.8	56.5	57.0	45.7	42.0	37.4	30.8	46.6
WBMS	50.7	54.9	56.2	47.5	41.2	34.9	28.5	44.8
JMV	51.4	56.0	55.2	51.6	42.3	35.5	26.4	45.5
DOMS	7.7	9.5	10.1	-7.0	-5.3	-6.4	1.0	1.4
BBMS	76.4	61.2	54.8	-11.5	10.6	5.0	15.7	30.3
%G*, SPE9PR "Drift" Scenario								
JMS	65.4	69.0	68.4	52.6	50.0	46.3	44.5	56.6
WBMS	63.7	68.0	66.9	53.5	48.1	41.8	39.5	54.5
JMV	29.2	22.7	21.9	-33.9	-42.8	-52.9	10.3	-6.5
DOMS	-1.4	9.4	12.0	-10.7	-4.5	-8.5	2.7	-0.1
BBMS	19.4	33.8	31.0	-7.6	1.1	-3.0	6.7	11.6
%G ^{xval} , SPE9PR "Drift" Scenario								
JMS	95.0	85.5	78.7	22.8	18.8	14.4	38.5	50.5
WBMS	94.7	84.1	77.3	16.8	5.0	-5.9	34.9	43.8
JMV	-40.0	-25.2	-12.2	48.3	31.6	16.9	11.3	4.4
DOMS	16.4	10.1	9.1	-23.4	-23.5	-26.9	1.8	-5.2
BBMS	40.5	9.4	7.9	0.8	17.3	9.0	5.0	12.8

Table 8. Symmetric gains split by individual components - SPE9PR only (compare to Table 2). OPR=Oil Production Rate, WPR=Water Production Rate, GPR=Gas Production Rate, WIN=Water Injection Rate.

Model	OPR	WPR	E_{base}			Excess-Deficit				
			GPR	WIN	Average	OPR	WPR	GPR	WIN	Average
%G*, SPE9PR "Non-Drift" Scenario										
JMS	0.12	0.28	0.17	0.09	0.17	18.25	66.45	53.60	47.61	46.48
WBMS	0.12	0.28	0.17	0.09	0.16	17.78	62.08	52.43	47.03	44.83
JMV	0.10	0.29	0.16	0.09	0.16	6.67	74.50	43.74	56.24	45.29
DOMS	0.12	0.31	0.18	0.11	0.18	-6.88	0.68	21.64	-10.16	1.32
BBMS	0.12	0.30	0.16	0.10	0.17	-3.85	74.44	16.89	40.08	31.89
%G*, SPE9PR "Non-Drift" Scenario										
JMS	0.12	0.28	0.17	0.09	0.17	19.13	66.98	52.18	48.19	46.62
WBMS	0.12	0.28	0.17	0.09	0.16	18.32	62.60	51.07	47.39	44.85
JMV	0.10	0.29	0.16	0.09	0.16	6.92	75.74	43.12	56.23	45.50
DOMS	0.12	0.31	0.18	0.11	0.18	-6.56	0.46	21.94	-10.27	1.39
BBMS	0.12	0.30	0.16	0.10	0.17	-3.84	76.80	7.71	40.63	30.33
%G*, SPE9PR "Drift" Scenario										
JMS	0.28	0.30	0.45	0.13	0.29	49.97	24.13	119.73	32.54	56.59
WBMS	0.31	0.34	0.45	0.14	0.31	51.49	27.09	102.64	36.77	54.50
JMV	0.30	0.32	0.51	0.20	0.33	1.12	-6.18	26.99	-47.96	-6.51
DOMS	0.28	0.28	0.45	0.11	0.28	-20.24	-6.97	22.32	4.31	-0.15
BBMS	0.32	0.31	0.54	0.13	0.33	-4.18	-1.04	26.64	25.13	11.64
%G ^{xval} , SPE9PR "Drift" Scenario										
JMS	0.28	0.30	0.45	0.13	0.29	61.81	39.10	74.23	27.01	50.54
WBMS	0.31	0.34	0.45	0.14	0.31	59.11	34.21	60.51	21.51	43.84
JMV	0.30	0.32	0.51	0.20	0.33	2.15	9.15	19.51	-13.28	4.38
DOMS	0.28	0.28	0.45	0.11	0.28	0.81	-27.32	15.73	-10.09	-5.22
BBMS	0.32	0.31	0.54	0.13	0.33	2.55	4.67	20.74	23.36	12.83